Fusion Engineering and Design 215 (2025) 115021

Contents lists available at ScienceDirect

Fusion Engineering and Design

journal homepage: www.elsevier.com/locate/fusengdes

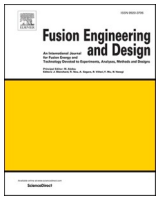

Numerical investigation of the DTT cryopump performance via 3D Direct Simulation Monte Carlo modeling

C. Tantos [a,*], H. Strobel [a], V. Hauer [a], C. Day [b], T. Giegerich [a], P. Innocente [c]

[a] Karlsruhe Institute of Technology, Hermann-von-Helmholtz-Platz 1, 76344 Eggenstein-Leopoldshafen, Germany
[b] Kyoto Fusioneering Europe, An der Raumfabrik 29, 76227 Karlsruhe, Germany
[c] Consorzio RFX, Corso Stati Uniti 4, 35127 Padova, Italy

ARTICLE INFO

Keywords:
Divertor tokamak test facility (DTT)
Vacuum pumping
DSMC method
Cryopump

ABSTRACT

DTT (Divertor Tokamak Test Facility) is a new facility, currently under construction in Frascati, Italy. The goal is to provide a basis to perform various scaled experiments for testing different magnetic configurations and alternative solutions for the power exhaust system of DEMO. The DTT pumping system design uses cryopumps as the primary pumping solution and up to 10 pumping openings. The cryopump system was developed at the Karlsruhe Institute of Technology (KIT). In the present work, the pumping capabilities of the DTT cryopump are estimated by performing a 3D numerical investigation of the neutral gas dynamics in the pumping duct of DTT including the entire complex cryopump geometry. The investigation is based on the Direct Simulation Monte Carlo (DSMC) method, which allows for a precise description of the neutral gas dynamics over the entire range of the gas collisionality. The values of the pumping probability for deuterium and neon were determined for two scenarios: open and closed divertor toroidal gaps. For open gaps, the probabilities were obtained as 0.4 for deuterium and 0.62 for neon, with a slight increase in both values observed when the gaps were closed. The results suggest that achieving the target of ten ports for deuterium pumping seems feasible, while for neon, partial elimination of toroidal leakages may be required. The importance of these simulations lies in the fact that, given the imposed simplifications, they delineate the existing pumping capabilities of the DTT particle exhaust and can act as a guide regarding the pumping capabilities among various plasma configurations. Moreover, this work demonstrates the level of geometric complexity that can be adopted in numerical modeling and highlights the effort needed to determine the values of the pumping probability, which are dependent on the chosen pumping technology.

1. Introduction

DTT (Divertor Tokamak Test Facility) [1,2] is a new facility currently under construction that will perform a series of scaled experiments to test different magnetic configurations and alternative solutions for the DEMO (DEMOnstration power plant) power exhaust system. The DTT facility has been tasked with the challenge of testing the science of alternative tokamak diversion concepts under integrated physical and technical conditions that can be reliably scaled up to DEMO.

During our preliminary 2D DTT divertor studies [3] a first assessment of the pumping capabilities of the DTT sub-divertor area was performed, for an ITER-like divertor assuming different plasma and pumping scenarios. The result of this work, in combination with the given geometric constraints, assisted in determining the location and size of the pumping aperture. Later, in our recent work [4], these preliminary studies were extended to a more stable and solidified divertor design, allowing a more detailed study. In [4], a very detailed 3D numerical analysis of the neutral gas dynamics inside the sub-divertor area of the DTT divertor has been performed for a given reference plasma scenario, namely, the DTT operation at the maximum additional power (P_{aux} = 45 MW) in partially detached condition achieved by neon impurity seeding. For an in-depth understanding of the computational domain and substructures in the divertor modeling from our previous work, see our recent divertor analysis [4]. The computational domain consisted only of the sub-divertor area, without including the pumping channel geometry and the actual geometry of the pumps, whose complex structures were replaced by the handshake parameter ξ, the so-called pumping probability. Thus, the performance of the divertor has

* Corresponding author.
E-mail address: christos.tantos@kit.edu (C. Tantos).

https://doi.org/10.1016/j.fusengdes.2025.115021
Received 11 January 2025; Received in revised form 6 March 2025; Accepted 27 March 2025
Available online 4 April 2025

been studied parametrically by considering different values of ξ. Based on the result of this analysis, the operational map of the DTT divertor as well as the conditions at the entrance of the pumping channel were determined as a function of the pumping probability ξ, which was considered as an open parameter.

The design of the DTT pumping system aims to use cryopumps as the main pumping solution and up to 10 pumping ports, with one cryopump assigned to each of the available ports [5]. The present work aims to perform a 3D numerical analysis of the performance of the DTT cryopump system covering the flow region from the entrance of the pumping ducts up to the cryopumps themselves, considering the very detailed design of the pumps. The present study links the relationship between the pumping probability concept applied in [3,4] with the established cryopump design. The current analysis is based on the Direct Simulation Monte Carlo (DSMC) method [6], which allows for a precise description of the neutral gas dynamics over the entire range of the gas collisionality. To achieve this, the DIVGAS workflow is employed, comprising three main steps: 1) preparation of the geometry and definition of boundary conditions, 2) the simulation itself, using one of the two kinetic approaches (DSMC or kinetic models) developed within DIVGAS [7], and 3) post-processing of the numerical results. Over the years, this workflow has proven to be a reliable and computationally efficient method for studying neutral gas dynamics in complex pumping systems.

The present paper is organized as follows. In Section 2, the examined 3D modeling domain is presented, and a detailed description of the applied boundary conditions is provided. In Section 3, a summary of the implemented DSMC numerical approach is given and all the values of the numerical parameters are defined. In Section 4, the numerical results are presented and discussed in detail, while Section 5 presents a summary of the present work, and the main findings are pointed out.

2. DTT CP model and boundary conditions

In this paragraph, a detailed description of the simulation domain and the applied boundary conditions are provided. An illustrative picture of the 3D simulated geometric configuration is shown in Fig. 1. The simulation domain consists of the triangular shaped vertical DTT pumping port and the main body of the DTT cryopump (CP). It is noted that, in DTT there are up to ten ports available for pumping, and each one is housing a cryogenic pump identical to the one depicted in Fig. 1.

In the present study, a very detailed representation of the CP design is used. As it is seen in Fig. 1, the main body of the CP consists of three main parts: 1) the baseplate which is the rear face of the CP shell, 2) a compound of 164 baffles with their main role being the heat protection of the cryopanels, the precooling of the gas in order to improve the gas adsorption process, and the condensation of the water vapor, and 3) the two coated cryosorption panels on which the gas adsorption process takes place. In addition, the frame tray is also included in the modeling, which acts as a guide-rail for the CP and at the same time helps to reduce heat losses due to the large temperature gradients between the port walls and the low-temperature environment of the CP.

In the modeling, the neutral deuterium and neon particles enter the computational domain from the pumping opening located on top of the pumping port, as indicated by the arrows in Fig. 1a. The incoming fluxes Φ_{in} for deuterium and neon have been extracted from the corresponding 3D divertor analysis in [4] and are applied here as boundary conditions. The imposed incoming fluxes correspond to a DTT Single Null (SN) reference scenario at the maximum additional power in partially detached condition achieved by neon impurity seeding [4]. To have a more realistic description of the incoming neutral fluxes distributions, the pumping opening area of 0.151 m^2 from which the neutral particles enter the present flow domain, is divided into two sub-surfaces, i.e.

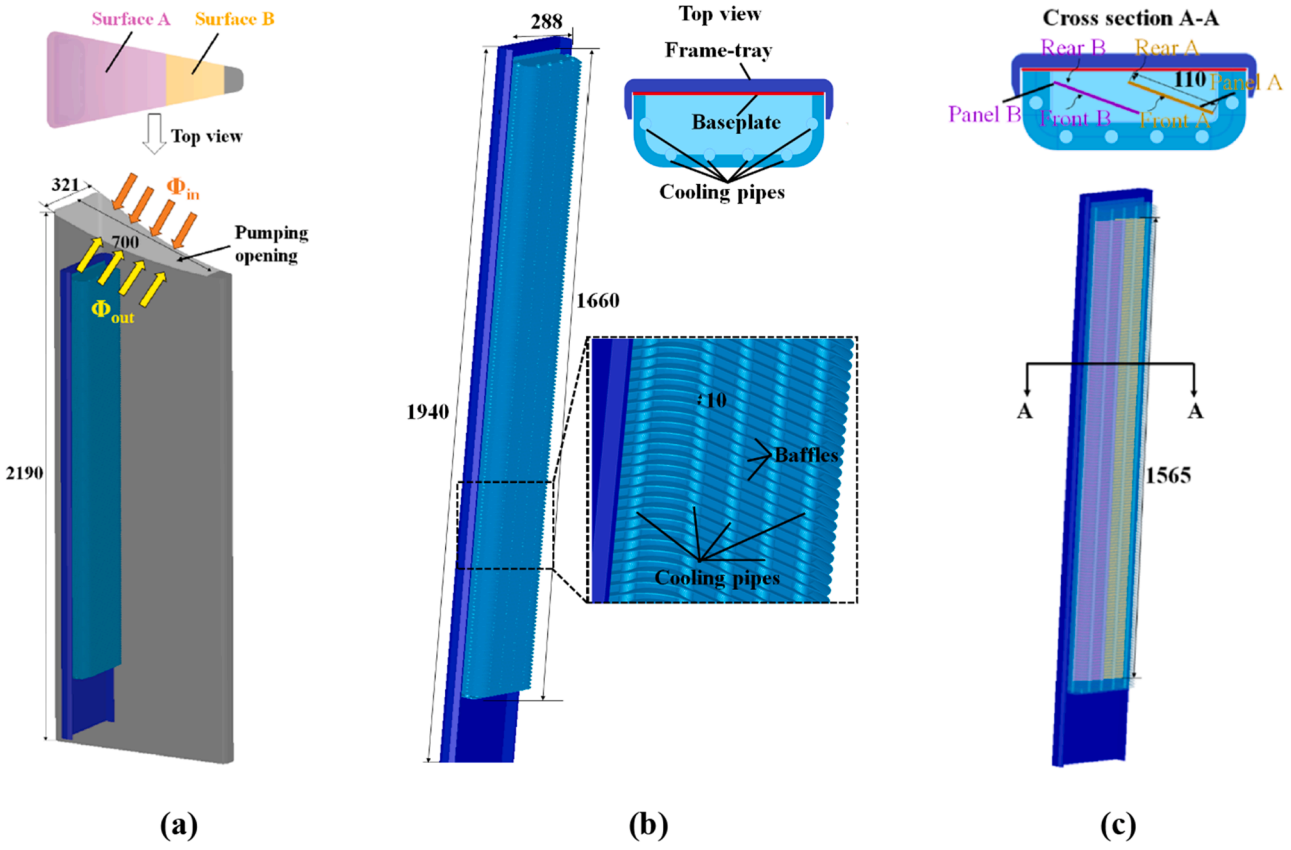

Fig. 1. a) 3D simulation model of the triangular shaped DTT pumping port with the CP installed in a vertical position; b) A more detailed illustration of the simulated design of the DTT CP; c) CP cryopanels on which the absorption process takes place and located between the 80 K baffles and the baseplate. All the dimensions are in millimetres (mm).

surface A and B with a total area of 0.121 m^2 and 0.0301 m^2 respectively (as shown in the top view in Fig. 1a). The values of the incoming fluxes are shown in Tables 1 and 2 for various scenarios with respect to the pumping probability ξ considered in [4]. In Table 1 the incoming fluxes for the worst scenario from pumping point of view are shown, where toroidal leakages are considered, while Table 2 shows the corresponding incoming fluxes for the most favourable case, where the divertor toroidal gaps are fully closed, and as it is shown leads to larger incoming fluxes. For a better understanding of the differences between the cases with and without toroidal leakages the reader is referred to Ref. [4]. The pumping probability ξ, which was treated as an open parameter in the divertor analysis conducted in [4], is defined as

$$\xi = 1 - \frac{\Phi_{out}}{\Phi_{in}}, \quad (1)$$

where Φ_{in} is the incoming flux at the pumping opening (given in Tables 1 and 2) and Φ_{out} is the particle flux formed in the opposite direction. It should be mentioned that the particle flux Φ_{out} is part of the incoming flux Φ_{in} which finally returns to the sub-divertor region. The net overall pumped flux through the pumping opening is obtained as $\Phi_{pumped} = \Phi_{in} - \Phi_{out}$.

In the modeling, after the neutral particles pass the upper opening surface of the pumping port they can move inside the internal volume of the port, colliding with the surrounding solid walls as well as with each other. Part of the particles passes through the narrow gaps between the baffles with a total vertical length of about 10 mm (see Fig. 1b). Then, the particles can be absorbed at the cryopanels assuming a sticking coefficient of 0.95 [8] and 1 [9] for deuterium and neon respectively. The adsorption process takes place at both rear and front faces of the two cryopanels (see Fig. 1c). The walls of the pumping port are maintained at 343 K, while the baffles, the cooling pipes and the baseplate are maintained at 80 K. The temperature of the frame tray is 315 K, and that of the cryopanels surfaces is 4.5 K. The applied temperatures correspond to a normal operational scenario and have been derived from the corresponding thermal analysis carried out during the design phase of the DTT CP. In the present model, the sticking coefficient is assumed to be independent of pressure and gas loading. We applied this simplistic assumption, since it has been successfully applied in similar Monte Carlo simulations of ITER CP [10,11] showing good agreement with experimental measurements [12]. It is noted that, by adding complexity to the description of the gas adsorption process, an increase in the modeling degrees of freedom and modeling parameters is expected, which may lead to an increase in modeling uncertainty rather than an improvement in the physical description, mainly due to the lack of experimental data needed for the determination of the open modeling parameters. In addition, the numerical results were obtained by assuming that particles—whether deuterium or neon—impinging on various components such as the inner walls of the port (including the bottom face of the port), cooling pipes, baffles, and frame tray, are re-emitted following diffuse scattering. Specifically, we modeled this re-emission using a half-Maxwellian distribution function, based on the corresponding surface temperature (i.e. with an energy accommodation coefficient of one). Thus, Φ_{out} represents the portion of the incoming flux that is not absorbed by the cryopanels.

Table 1
Incoming fluxes Φ_{in} through surfaces A and B for various values of the pumping probability ξ obtained from the divertor analysis in [4] for the scenario in which the divertor toroidal lekages are considered.

ξ		Surface A		Surface B	
Deuterium	Neon	Deuterium	Neon	Deuterium	Neon
0.3	0.3	1.78E+22	1.31E+20	8.85E+21	6.55E+19
0.4	0.4	1.63E+22	1.27E+20	8.15E+21	6.32E+19
0.4	0.6	1.64E+22	8.94E+19	8.18E+21	4.46E+19
0.4	0.65	1.64E+22	8.34E+19	8.18E+21	4.16E+19
0.45	0.45	1.57E+22	1.23E+20	7.85E+21	6.15E+19

Table 2
Incoming fluxes Φ_{in} through surfaces A and B for various values of the pumping probability ξ obtained from the divertor analysis in [4] in the case that the divertor toroidal leakages are not considered.

Ξ		Surface A		Surface B	
Deuterium	Neon	Deuterium	Neon	Deuterium	Neon
0.3	0.3	3.06E+22	2.54E+20	1.14E+22	9.50E+19
0.4	0.4	2.66E+22	2.29E+20	9.93E+21	8.57E+19
0.42	0.4	2.59E+22	2.35E+20	9.66E+21	8.79E+19
0.42	0.55	2.59E+22	1.72E+20	9.69E+21	6.42E+19
0.42	0.65	2.69E+22	1.46E+20	9.69E+21	5.44E+19
0.42	0.67	2.60E+22	1.41E+20	9.72E+21	5.28E+19
0.5	0.5	2.34E+22	2.06E+20	8.74E+21	7.70E+19

3. Applied numerical method and numerical parameters

In the present study, the neutral gas flow behaviour is simulated based on the DSMC method [6]. The DSMC method allows accurate modeling of the neutral gas dynamics covering the entire range of the gas collisionality, making it the optimal choice for studying the present flow configuration. DSMC is a particle-based numerical technique and is considered by many researchers as a simplified Molecular Dynamics method for solving the time-dependent, nonlinear Boltzmann equation. A very detailed description of the applied DSMC algorithm can be found in [7]. Thus, only a brief description of the DSMC method is provided here. The key idea of the method is to track a large number of statistically representative particles. The physical space is discretized into cells, which are used to track particles and calculate the bulk properties. Macroscopic quantities are calculated at the center of each cell by properly combining the properties of computational particles. The particles move according to Newton's laws and collide with each other conserving mass, momentum, and energy. The particles' motion is calculated deterministically but the collisions are treated statistically. In the present work the collisions between the particles are simulated based on the No-Time-Counter (NTC) scheme [6,13], supplemented by the Variable Hard Sphere (VHS) model [13]. The internal energy exchange during binary collisions of diatomic molecular deuterium among the gas mixture was modeled based on the phenomenological Larsen-Borgnakke (LB) model [14]. The viscosity indexes of deuterium and neon are taken equal to ω=0.750 and 0.786 respectively, with the corresponding VHS model diameters being 0.303 nm and 0.289 nm. Such a choice of the VHS parameters ensures a good description of the experimental viscosity values [15,16] in a wide range of the gas temperature from 30 K up to 300 K, with the maximum deviation being within 6 %. The average number of particles in each simulation ranges between 300×10^6 and 500×10^6. The number of grid cells is equal to 10 millions in all simulations. The time step of $\Delta t = 1$ μs is chosen to be sufficiently smaller than the cell traversal time in order to avoid light particles flying long distances. This number assures that the statistical scattering of macroscopic quantities along the computational domain is sufficiently low. In order to reduce the relative statistical scattering of the macroscopic quantities to less than 5 %, the macroscopic quantities have been obtained by time averaging over 3×10^6 time steps. The simulations of this work were performed on the MARCONI High-Performance Computing system [17] using 1024 cores for each run, and the typical time for reaching steady state conditions was approximately three days for each case.

4. Results and discussion

In this section, the obtained numerical results are presented and discussed. In Fig. 2a, the deuterium incoming flux is plotted as a function of the pumping probability ξ for the two limit divertor pumping scenarios assumed in the divertor analysis in [4], i.e. where the toroidal

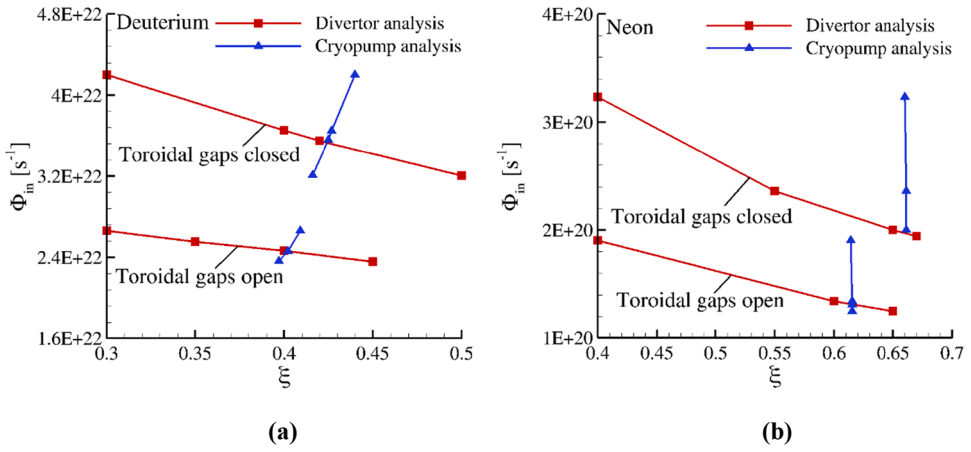

Fig. 2. Overall incoming flux Φ_{in} vs. pumping probability ξ for deuterium with the divertor toroidal gaps a) open and b) closed.

gaps are a) fully open and b) fully closed. The results obtained from the divertor analysis as well as those obtained from the present CP analysis are shown in the same figure. It is noted that, in the divertor analysis [4], the pumping probability ξ is an input parameter and the incoming flux to the pumping duct is obtained as part of the solution, while in the present work the pumping probability ξ is obtained as part of the solution. In other words, ξ is determined by the pumping capability of the present DTT CP technology for the defined range of the incoming flux extracted from the divertor analysis in [4]. The results from the current CP analysis indicate that the pumping probability ξ exhibits only a small variation within the considered range of incoming fluxes. The values of the pumping probability ξ are determined at the point where the two curves from the divertor and CP analyses intersect, ensuring that the overall particle flux balance between the sub-divertor and pumping duct regions is maintained. For the two limit pumping scenarios, i.e. when the toroidal gaps are open and closed, the deuterium pumping probability ξ is 0.40 and 0.42, respectively. In Fig. 2b, the corresponding results for neon are shown. All the points for the divertor analysis in Fig. 2b correspond to the same value of the deuterium pumping probability ξ as those obtained in Fig. 2a (0.40 and 0.42 for the two limit pumping scenarios). In that way, a simultaneous individual particle flux balance for both deuterium and neon at the pumping opening is achieved. From Fig. 2b, it can be deduced that the corresponding values of the pumping probability ξ for neon are 0.62 and 0.66 respectively. It should be emphasized that the deuterium curves in Fig. 2a from the divertor analysis are unaffected by any changes in the neon pumping probability, due to the low neon mole fraction (<2 %) in the sub-divertor region. In contrast, the corresponding neon curves in Fig. 2b are significantly influenced by variations in the deuterium pumping probability.

With the values of the pumping probability for deuterium and neon known, the effective pumping speed at the pumping opening can be easily determined from Fig. 3, where the effective pumping speeds of deuterium and neon are plotted as a function of the pumping probability ξ. The effective pumping speed S_P at the pumping opening was calculated in [4] as follows:

$$S_P = \frac{\Phi_{pumped}(\xi)}{\bar{n}(\xi)}, \tag{2}$$

where $\Phi_{pumped}(\xi)$ is the pumped flux and $\bar{n}(\xi)$ is the average number density across the pumping opening.

The results shown in Fig. 3 indicate that in the worst-case scenario from pumping point of view (when the divertor toroidal gaps are open), the effective pumping speeds for deuterium and neon are 28.5 m^3/s and 24 m^3/s, respectively, when the pumping probabilities $(\xi_{deuterium},\ \xi_{neon})$ are set to $(0.4,\ 0.62)$. In the most favorable scenario (when the divertor toroidal gaps are closed), the corresponding effective pumping speeds

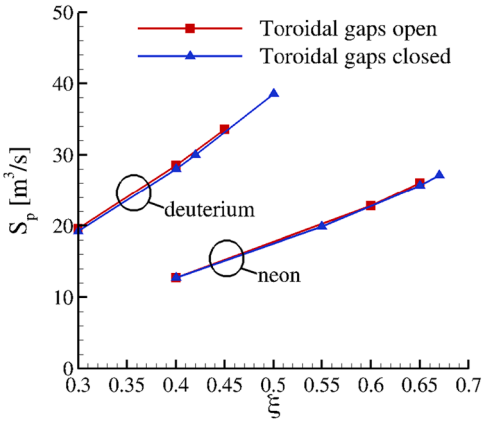

Fig. 3. Overall incoming flux Φ_{in} vs. pumping probability ξ for deuterium with the divertor toroidal gaps a) open and b) closed.

with $(\xi_{deuterium},\ \xi_{neon}) = (0.42,\ 0.66)$, are 30 m^3/s and 26.4 m^3/s, respectively.

Using the calculated pumping probability values (ξ) for deuterium and neon, the total torus pumped flux, denoted as $\Gamma_{pumped} = \Phi_{pumped} \times$ No. of ports, can be estimated. This helps in gaining a better understanding of the overall pumping performance in relation to both pumping constraints and requirements. The current design of the pumping system plans to use half of the available openings for pumping, i.e., 9 to 10 out of the 18 total openings [5]. The decision regarding the number of ports involves multiple factors and engineering constraints, aiming to balance pumping requirements with other port functions. Under steady-state conditions, the total puffing fluxes for the plasma scenario under consideration are $\Gamma_{puffing,\ deuterium} = 8.4E22\ s^{-1}$ and $\Gamma_{puffing,\ neon} = 1E21\ s^{-1}$, and these should match the overall torus pumped flux, Γ_{pumped}. Fig. 4 presents the total torus pumped flux for the two pumping scenarios (toroidal gaps open and closed) as a function of the number of pumping ports. It is noted that the torus pumped fluxes shown in this figure are based on the pumping probabilities for the two species per port calculated from the present study, namely, $(\xi_{deuterium},\ \xi_{neon}) = (0.4,\ 0.62)$ and $(\xi_{deuterium},\ \xi_{neon}) = (0.42,\ 0.66)$. Although the pumping probabilities for the two scenarios are quite similar, the overall pumped fluxes differ significantly due to the large disparity in the incoming fluxes (see Tables 1 and 2). As shown in Fig. 4, the minimum number of openings required for deuterium in the worst-case scenario (with toroidal gaps open) is nine, which meets the 10-port restriction. However, significantly greater flexibility is achieved when the divertor toroidal openings are fully closed, particularly for

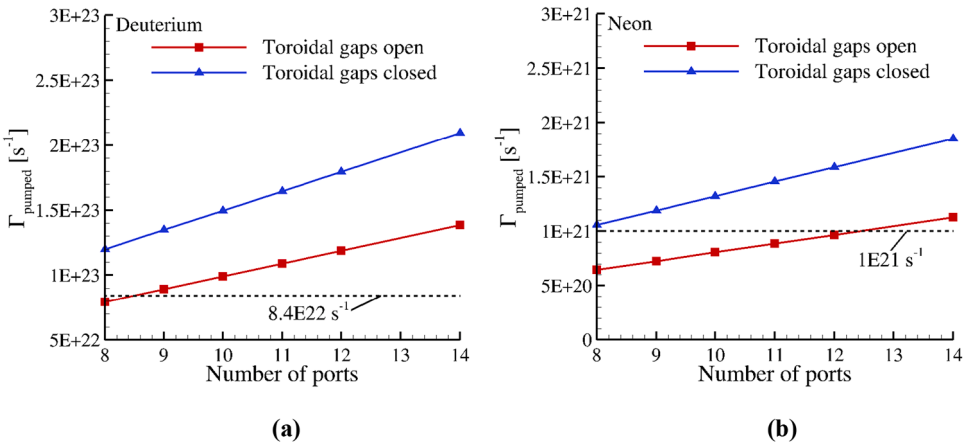

Fig. 4. Overall torus pumped flux Γ_{pumped} vs. number of pumping ports for deturium (a) and neon (b). The dashed lines correspond to the pumping requirements, i.e. $\Gamma_{puffing,\ deuterium} = 8.4E22\ s^{-1}$ and $\Gamma_{puffing,\ neon} = 1E21\ s^{-1}$.

neon, where it is also necessary to partially eliminate toroidal leakage to achieve the 10-port restriction. Additional simulations demonstrated that reducing the sticking coefficient on the cryopanels by 10 % results in less than a 1 % variation in the pumping probability values ξ at the pumping opening, and consequently, in the overall torus pumped fluxes shown in Fig. 4.

In Table 3, the distribution of the overall neon and deuterium incoming flux Φ_{in} on the rear and front surfaces (see Fig. 1c) of the two cryopanels A and B is shown. As expected, a larger portion of the incoming flux is absorbed on the front surfaces of both panels compared to the rear surfaces. When comparing the fluxes on the front surfaces of the two panels, it is evident that the front surface of panel B absorbs higher fluxes. This behavior can be attributed to the arrangement of the two panels. The front surface of panel B is the first absorption surface encountered by the neutral particles as they pass through the narrow regions between the baffles and enter the main CP area. The distributions of the incoming flux for the two pumping scenarios (toroidal gaps open and closed) are very similar, with the percentages for the scenario with the toroidal gaps closed being slightly higher than those for the scenario with the toroidal gaps open. This behaviour reflects the slight deviations in the calculated values of the pumping probability ξ for the two pumping scenarios. The last two rows of Table 3, show the data for the pumping scenario with the divertor toroidal gaps completely open imposing a reduction of 10 % in the sticking coefficients on the cryopanels (i.e. the sticking coefficents for this case are 0.85 for deuterium and 0.9 for neon). Overall, on the front surfaces of the panels, where the highest pumped fluxes are observed, the decrease in pumped fluxes due to the reduction in the sticking coefficient is minimal, remaining below 1 %. This means that the obtained values of the pumping probability ξ are not highly sensitive to the small changes in the sticking coefficients, highlighting the expected good performance of the CP even during the initial stage of the saturation phase of the cryopanels during one operation cycle (1 day). The dependence of sticking coefficient on pumped amount is known to be rather weak up to about 80 % of the capacity limit, and then showing a strong decrease. It should be noted that the remaining fraction of the incoming flux, which is not adsorbed on the front and rear surfaces of the cryopanels, represents the particle flux returning to the sub-divertor area.

Table 3
Distribution of the overall neon and deuterium incoming flux Φ_{in} on the rear and front surfaces (see Fig. 1c) of the two cryopanels A and B.

Scenario	Species	Cryopanel surface			
		Front A	Rear A	Front B	Rear B
Toroidal gaps open	Deuterium	13.8 %	4.54 %	19.4 %	2.46 %
	Neon	21.7 %	6.71 %	29.9 %	3.14 %
Toroidal gaps closed	Deuterium	14.7 %	4.82 %	20.6 %	2.53 %
	Neon	23.5 %	7.22 %	32.3 %	3.17 %
Toroidal gaps open**	Deuterium	13.6 %	4.59 %	19.2 %	2.78 %
	Neon	21.5 %	6.73 %	29.6 %	3.53 %

**Assuming 10 % reduction in the sticking coefficients on the cryopanels, i.e. 0.85 for deuterium and 0.9 for neon.

In Fig. 5, the distributions of the overall deuterium and neon pumped fluxes along the front and rear surfaces of the two cryopanels A and B are shown. The results in Fig. 5 correspond to the scenario assuming the divertor toroidal gaps open. The cryopanel surfaces were divided into five equally-sized partitions and the partial pumped flux at each partition was calculated. A non-uniform distribution of the pumped flux is observed, and, as expected, the highest values are always reached at the partition closest to the pumping opening of the divertor (i.e. partition 1). More specifically, the pumped flux in partition 1 accounts for about 10–15 % of the total CP flux (as shown in Panel A and Panel B). However, this percentage significantly decreases to 5–6.5 % in partition 5, which is the partition farthest from the pumping opening. It has also been observed that the distributions of the neon-pumped fluxes are similar to those of deuterium. Notably, the quantitative (within 2 %) and qualitative observations regarding the pumped flux distributions, as mentioned above, still hold true for the fully closed divertor gap scenario.

Fig. 6 shows the 2D flow-fields of the overall pressure, temperature and Knudsen number on the vertical cross section A-A (as indicated in the bottom right corner of the subfigures). To gain a deeper understanding of the evolution of the corresponding flow fields in the third dimension, Fig. 7 presents several 2D horizontal contour plots at different cross-sections along the *y*-axis. The Knudsen number is defined as [6]:

$$Kn = \frac{1}{D_h}\sum_{i=1}^{2}\frac{n_i}{n}\left[\sum_{j=1}^{2}\pi d_{ij}^2 n_j\left(\frac{T_{ref}}{T}\right)^{\omega_{ij}-0.5}\sqrt{1+\frac{m_i}{m_j}}\right]^{-1}, \quad (3)$$

where $D_h = 0.333m$ is the hydraulic diameter of the pumping opening, n_j is the local number density of the j species, d_{ij} are the average VHS diameter of the species i and j, T is the temperature, and m is the mass of the corresponding species. In Eq. (3), T_{ref}=300 K is the reference temperature and ω is the viscosity index. The contours in Figs. 6 and 7, correspond to the operational point for the 2 pumping scenarios: one with divertor toroidal leakages and one without. Specifically, the scenarios are defined by $(\xi_{deuterium}, \xi_{neon}) = (0.4, 0.62)$ and $(\xi_{deuterium}, \xi_{neon}) = (0.42, 0.66)$. Strong pressure gradients are observed in the pumping duct area. In the pumping scenario with the divertor toroidal gaps open, the pressure drops from an average value of 1.74 Pa near the pumping opening to 0.6 Pa at the bottom of the pumping duct. In the

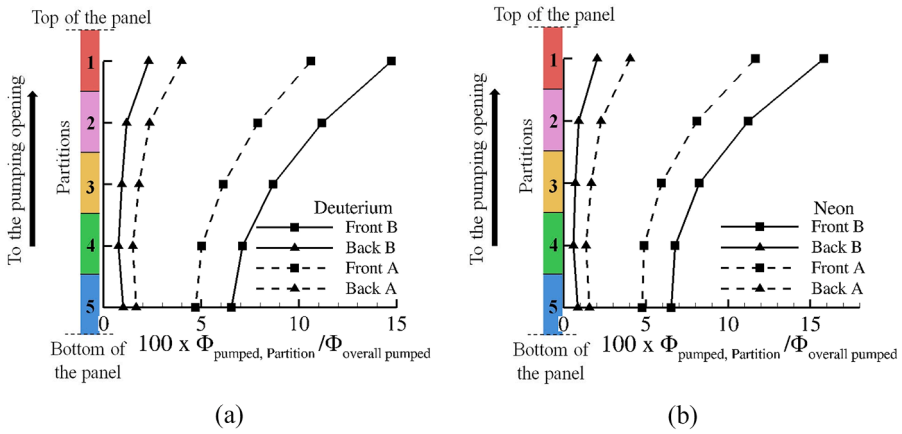

Fig. 5. Distribution of the overall pumped flux per port on five equal-sized partitions (Each partition is 0.313 m long) of the panels A and B for deuterium (a) and neon (b) (Scenario: Toroidal gaps open).

pumping scenario with the divertor toroidal gaps closed, the pressure within the pumping duct is maintained at higher values, ranging from 0.94 Pa (at the bottom) to 2.47 Pa (near the pumping opening), compared to the scenario with the toroidal gaps open. However, the pressure reduction is quantitatively similar in both cases, with a decrease of approximately 62 %. This reduction in pressure corresponds to a significant decrease in the pumped flux (ranging from about 48 % to 61.5 %, depending on the panel face and the examined scenario) between partition 5, which is near the pumping opening, and partition 1, located at the bottom of the CP (see Fig. 5). As expected, the pressure inside the pump is maintained at even lower values for both pumping scenarios. More specifically, in the pumping scenario with the divertor toroidal gaps open, the pressure in the area between the baffles and the front faces of the cryopanels ranges from 0.049 Pa (at $y = 0.5$ m) to 0.20 Pa (at $y = 1.854$ m). In the region between the two cryopanels at the same y-positions, the corresponding pressure values are 0.014 Pa and 0.16 Pa, respectively. In the pumping scenario with the divertor toroidal gaps closed, the pressure in the region between the baffles and the front faces of the cryopanels ranges from 0.078 Pa to 0.27 Pa. Meanwhile, in the area between the two cryopanels, the pressure ranges from 0.022 Pa to 0.21 Pa. The temperature flow-fields for the two pumping scenarios are found to be quite similar. The neutral gas inside the pumping duct remains at a temperature which is close to that of the duct walls (T = 343 K), while a sharp decrease in temperature is observed in the region near the baffles. The gas temperature decreases from its high value of 343 K inside the pumping duct to about 135 K in front of the baffles. A further reduction of approximately 80 K is observed as the gas moves through the regions between the baffles. The neutral gas temperature inside the CP remains low between 55 and 65 K. The strong gradients in the gas pressure and temperature result in a strong variation in the Knudsen number inside the whole computational domain. The obtained Knudsen number values indicate that flow varies from slip regime inside the pumping duct to the transition regime inside the CP. In this range the neutral-neutral collisions play a very significant role, and their omission would lead to inaccurate results. Furthermore, to evaluate the assumption of the complete energy accommodation coefficient implemented in the present work, we conducted additional simulations using the more advanced Cercignani–Lampis model [18] under the worst-case scenario with toroidal gaps open. This model enables a more accurate description of energy exchange during gas-surface interactions through the definition of an energy accommodation coefficient. Although experimental data on the energy accommodation coefficient are limited and exhibit variability across different experimental measurements, we assumed a value of 0.1 for the coefficient associated with the normal motion of deuterium particles at high-temperature surfaces (such as the inner walls of the port and the frame tray) and a higher value of 0.25 for the 80 K panels. This choice seems reasonable by combining experimental data reported in the literature for various surface materials [19–20]. The results showed that such a significant change in the energy accommodation coefficient results in only a small variation in the pumping probability (around 3 %) and the pressure inside the port (around 5 %). However, the temperature around the baffles was more sensitive to the choice of energy accommodation coefficient, with the maximum observed deviations in temperature and pressure inside the cryopump region, compared to full energy accommodation, remaining below 10 % and 5 %, respectively.

5. Conclusions

In the present work, a 3D numerical study of neutral gas dynamics in the pump duct of DTT, incorporating the full complexity of the CP geometry, is conducted using the Direct Simulation Monte Carlo (DSMC) method. This approach provides a detailed description of the neutral gas dynamics across the full range of gas collisionality. The neutral particle flux input used in the present study was obtained from our recent 3D divertor analysis and includes two limiting cases regarding the consideration of divertor toroidal leakages. The relationship between the concept of pumping probability, which has been widely applied in the past, and the response of real pumping technology is revealed. For the worst-case scenario (divertor toroidal gaps open), the pumping probabilities for deuterium and neon were obtained equal to 0.4 and 0.62 respectively, with the corresponding effective pumping speeds at the entrance of the pumping ports being 28.5 m^3/s and 24 m^3/s respectively. For the most favourable scenario (divertor toroidal gaps closed) slightly higher values of the pumping probability and effective pumping speed were obtained, namely $(\xi_{\text{deuterium}}, \xi_{\text{neon}}) = (0.42, 0.66)$, and $(S_{P,\text{deuterium}}, S_{P,\text{neon}}) = (30\ m^3/s, 26.4\ m^3/s)$. The results indicate that the pumping probabilities are only negligibly affected by a 10 % reduction in the capture coefficients on the cryopanels. This underscores the expected high performance of the CP, even during the initial stage of the saturation phase of the cryopanels in a single operational cycle. For deuterium pumping, the requirement of 10 available ports is satisfied even for the worst-case scenario (toroidal gaps open) but keeping this number of ports may allow for more flexibility with respect to other plasma scenarios, while in the case of neon pumping toroidal leakages seem necessary to be partially eliminated. The strong pressure and temperature gradients inside the present flow domain result to a strong variation of the Knudsen number from transition up to slip regime, which can be accurately described by the implemented DSMC method.

The results presented in this work are based on several simplifications, including assumptions made in plasma modeling, divertor analysis, and the assumption that the sticking coefficient of each gas is

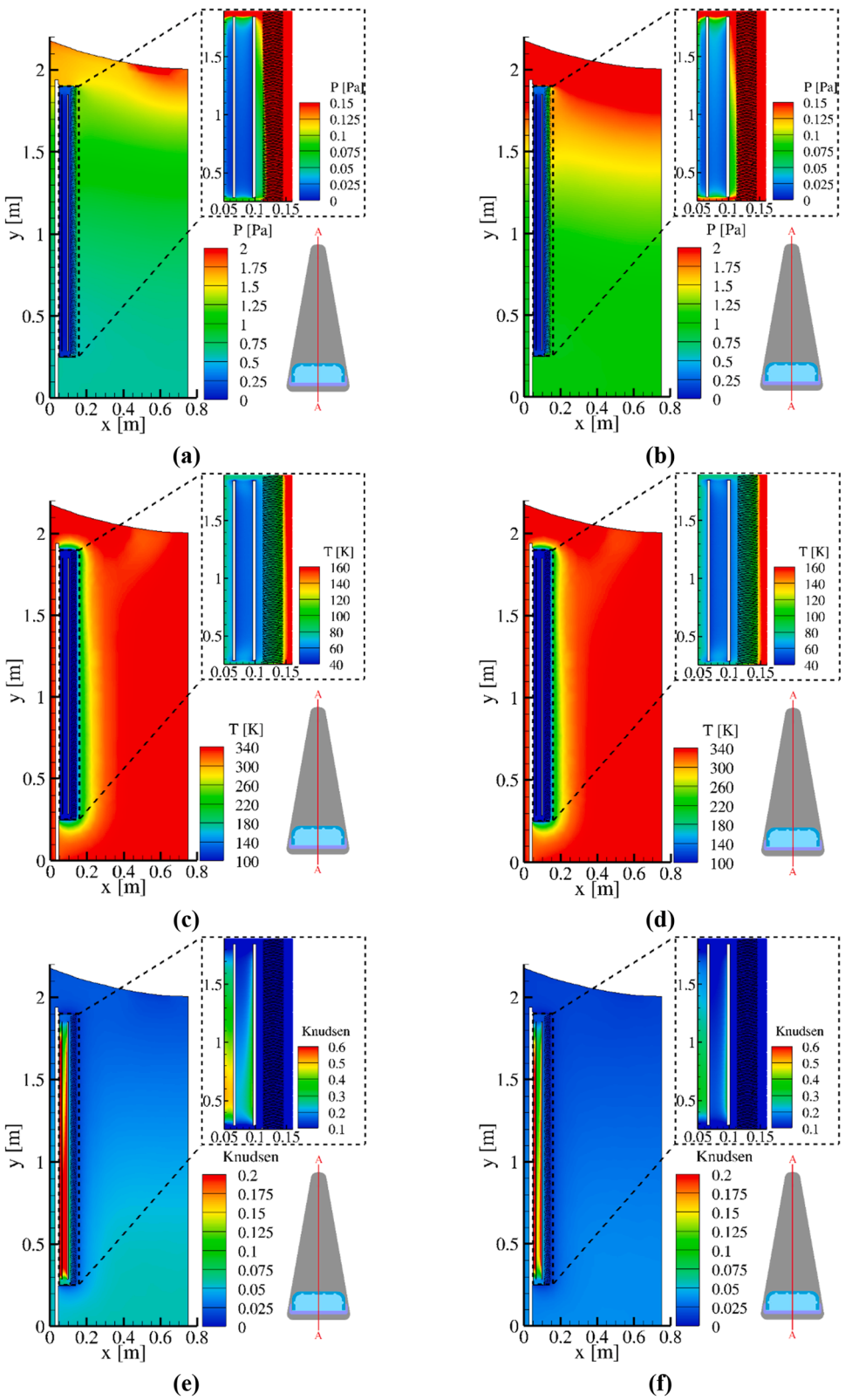

Fig. 6. 2D vertical cross section contour plots (cross section A-A) of the overall pressure (a,b), temperature (c,d) and Knudsen number (e,f) for the two limit scenarios, namely, divertor toroidal gaps open (a,c,e) and closed (b,d,f).

independent of pressure and gas loading. It is hoped that once the DTT is operational, the impact of these assumptions can be thoroughly evaluated allowing for further improvements in the modeling at a later stage. Overall, this work shows the level of geometrical complexity that can be adopted in the numerical modeling and highlights the effort needed to determine the values of the pumping probability, which are dependent on the chosen pumping technology.

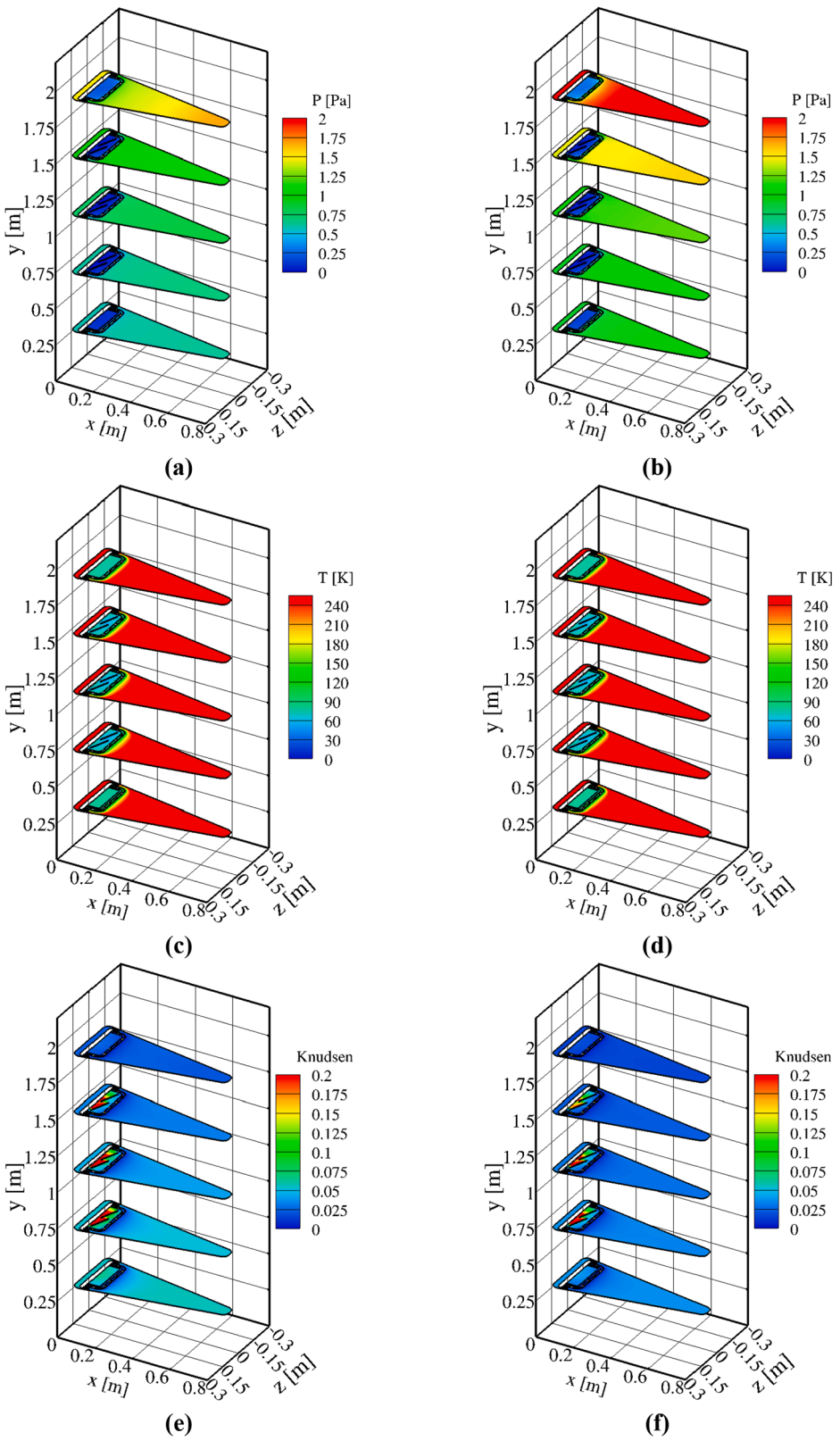

Fig. 7. 2D horizontal contours in several cross sections along the y-axis of the overall pressure (a,b), temperature (c,d) and Knudsen number (e,f) for the two limit scenarios, namely, divertor toroidal gaps open (a,c,e) and closed (b,d,f).

CRediT authorship contribution statement

C. Tantos: Writing – review & editing, Writing – original draft, Visualization, Software, Methodology, Investigation, Formal analysis, Data curation, Conceptualization. **H. Strobel:** Writing – review & editing, Visualization, Software, Data curation. **V. Hauer:** Writing – review & editing, Methodology, Investigation, Formal analysis. **C. Day:** Writing – review & editing, Writing – original draft, Project administration,

Methodology, Investigation, Formal analysis, Conceptualization. **T. Giegerich:** Project administration. **P. Innocente:** Writing – review & editing, Writing – original draft, Visualization, Validation, Project administration, Investigation, Formal analysis.

Declaration of competing interest

The authors declare that they have no known competing financial interests or personal relationships that could have appeared to influence the work reported in this paper.

Acknowledgments

This work has been carried out within the framework of the EUROfusion Consortium, funded by the European Union via the Euratom Research and Training Programme (Grant Agreement No 101052200—EUROfusion). Views and opinions expressed are however those of the author(s) only and do not necessarily reflect those of the European Union or the European Commission. Neither the European Union nor the European Commission can be held responsible for them. In addition, this work was performed within the 8th cycle of MARCONI-FUSION HPC (Project TOK-KIT) and also partially on the HoreKa supercomputer (Project ngdsim) funded by the Ministry of Science, Research and the Arts Baden-Württemberg and by the Federal Ministry of Education and Research. Moreover, we acknowledge support by the KIT Publication Fund of the Karlsruhe Institute of Technology.

Data availability

Data will be made available on request.

References

[1] R. Albanese, A. Pizzuto, WPDTT2 Team, DTT project proposal contributors, the DTT proposal. A tokamak facility to address exhaust challenges for DEMO: introduction and executive summary, Fusion Eng. Des. 122 (2017) 274–284, https://doi.org/10.1016/j.fusengdes.2016.12.030.

[2] R. Albanese, with the support of the DTT community, DTT - Divertor Tokamak Test facility: a testbed for DEMO, Fusion Eng. Des. 167 (2021) 112330, https://doi.org/10.1016/j.fusengdes.2021.112330.

[3] C. Tantos, S. Varoutis, C. Day, L. Balbinot, P. Innocente, F. Maviglia, DSMC simulations of neutral gas flow in the DTT particle exhaust system, Nucl. Fusion 62 (2022) 026038, https://doi.org/10.1088/1741-4326/ac42f5.

[4] C. Tantos, S. Varoutis, V. Hauer, C. Day, P. Innocente, 3D numerical study of neutral gas dynamics in the DTT particle exhaust using the DSMC method, Nucl. Fusion 64 (2024) 016019, https://doi.org/10.1088/1741-4326/ad0c80.

[5] F. Romanelli, et al., Divertor Tokamak Test facility project: status of design and implementation, Nucl. Fusion 64 (2024) 112015, https://doi.org/10.1088/1741-4326/ad5740.

[6] G.A. Bird, Molecular Gas Dynamics and Direct Simulation of Gas Flows, Clarendon Press, Oxford, 1994.

[7] C. Tantos, S. Varoutis, C. Day, Deterministic and stochastic modeling of rarefied gas flows in fusion particle exhaust systems, J. Vac. Sci. Technol. B 38 (2020) 064201, https://doi.org/10.1116/6.0000491.

[8] C. Day, Basics and applications of cryopumps, in: CAS - CERN Accelerator School: Vacuum in Accelerators 241, 2007. https://api.semanticscholar.org/CorpusID:43385190.

[9] M. Scannapiego, C. Day, Experimental investigation on charcoal adsorption for cryogenic pump application, Conf. Ser. Mater. Sci. Eng. 278 (2017) 012160, https://doi.org/10.1088/1757-899X/278/1/012160.

[10] S. Varoutis, C. Day, Numerical modeling of an ITER type cryopump, Fusion Eng. Des. 87 (2012) 1395–1398, https://doi.org/10.1016/j.fusengdes.2012.03.023.

[11] M. Kovari, R. Clarke, T. Shephard, Compound cryopump for fusion reactors, Fusion Eng. Des. 88 (2013) 3293–3298, https://doi.org/10.1016/j.fusengdes.2013.10.009.

[12] X. Luo, C. Day, H. Haas, S. Varoutis, Experimental results and numerical modeling of a high-performance large-scale cryopump. I. Test particle Monte Carlo simulation, J. Vac. Sci. Technol. A 29 (2011) 041601, https://doi.org/10.1116/1.3585665.

[13] C. Shen, Rarefied Gas Dynamics: Fundamentals, Simulations and Micro Flows, Springer, 2005.

[14] C. Borgnakke, P.S. Larsen, Statistical collision model for Monte Carlo simulation of polyatomic gas mixture, J. Comput. Phys. 18 (4) (1975) 405–420, https://doi.org/10.1016/0021-9991(75)90094-7.

[15] J. Kestin, K. Knierim, E.A. Mason, B. Najafi, S.T. Ro, M. Waldman, Equilibrium and transport properties of the noble gases and their mixtures at low density, J. Phys. Chem. Ref. Data 13 (1984) 229, https://doi.org/10.1063/1.555703.

[16] M.J. Assael, S. Mixafendi, W.A. Wakeham, The viscosity of normal deuterium in the limit of zero density, J. Phys. Chem. Ref. Data 16 (2) (1987) 189, https://doi.org/10.1063/1.555778.

[17] https://www.hpc.cineca.it/systems/hardware/marconi/.

[18] C. Cercignani, M. Lampis, Kinetic models for gas-surface interactions, Transp. Theory Stat. Phys. 1 (2) (1971) 101–114, https://doi.org/10.1080/00411457108231440.

[19] Yu.G. Semyonov, S.F. Borisov, P.E. Suetin, Investigation of heat transfer in rarefied gases over a wide range of Knudsen numbers, Int. J. Heat Mass Transf. 27 (1984) 1789, https://doi.org/10.1016/0017-9310(84)90161-3.

[20] F. Sharipov, G. Bertoldo, Heat transfer through a rarefied gas confined between two coaxial cylinders with high radius ratio, J. Vac. Sci. Technol. A 24 (2006) 2087–2093, https://doi.org/10.1116/1.2353847.